

## Gas Laser with Saturable Absorber. I. Single-Mode Characteristics

Rainer Salomaa and Stig Stenholm

*University of Helsinki, Research Institute for Theoretical Physics, Siltavuorenpenger 20 B, SF-00170, Helsinki, 17, Finland*

(Received 26 February 1973)

This paper discusses the case of a Doppler-broadened gas laser with a saturable intracavity absorber gas. The semiclassical equations governing the field intensities and the atomic density-matrix elements are set up. The latter are written as Fourier series, the components of which are shown to obey coupled difference equations. In this paper the exact steady-state solution in single-mode operation is obtained. The lowest approximation (rate-equation approximation) is used to compute detailed characteristics of the system. In particular, the influence of the pumping rates in the two cells are investigated and displayed in the figures. The regions of bistable operation are determined and conditions for the occurrence of an inverted Lamb dip are given. The effect of a slow modulation of the pumping rates is discussed. The range of validity of the lowest approximation is investigated both analytically and numerically. Finally, there is a brief discussion of the influence of pressure on the parameters of the theory.

### I. INTRODUCTION

In several recent experiments a nonlinearly absorbing material has been saturated by laser light. The largest field intensities are achieved when the absorber is placed directly inside the optical cavity of the laser. Then, however, the operation of the laser is drastically affected and acquires new features that are of interest in their own right. These phenomena are mainly governed by the properties of the absorber and provide means for its exploration.

Lee, Schoefer, and Barker<sup>1</sup> were able to induce strong coupling between the modes of a He-Ne laser (0.6328  $\mu\text{m}$ ) with an intracavity cell containing Ne gas at a lower pressure than in the amplifier cell. With large enough absorption, single-mode operation was maintained over the whole tunable region. The power losses due to the absorber were remarkably small. A major fraction of the total multimode power without absorption was obtained in the surviving mode. When the pumping of the absorption cell exceeded 90% of the value needed to extinguish the oscillation totally, the laser system displayed hysteresis: If interrupted, the oscillation did not start again.

Lisitsyn and Chebotaev<sup>2</sup> performed experiments similar to those of Lee *et al.* In the place of the Lamb dip they observed an inverted Lamb dip of the homogeneous width in the absorber cell. They used this to measure the pressure effects on the decay rates of the Ne atoms in different He-Ne mixtures. In another paper<sup>3</sup> they report observations of the hysteresis effects: A detuning was found to cut off the oscillation discontinuously when the absorption was large.

Several applications of the saturable absorber laser have been discussed: Mode selection is

studied in Refs. 1, 4, and 5. The inverted Lamb dip provides the basis for an extremely stable frequency standard; see, e.g., Refs. 6 and 7. Mode locking is achieved in regions where it does not occur in ordinary lasers (Fox *et al.*<sup>8</sup>). The absorber can be used for Q switching and bistable logic (Szöke *et al.*<sup>9</sup>). Perhaps the most successful and scientifically interesting application is in the field of nonlinear spectroscopy; see, e.g., Refs. 2, 7, and 10.

The theory of a saturable absorber was discussed by Feld, Javan, and Lee<sup>11</sup> and Kazantsev, Rautian, and Surdutovich<sup>12</sup> within the framework of a perturbative approach. When the pressure in the amplifier cell exceeds that of the absorber cell, the latter is saturated more efficiently and the oscillating mode is found to be strongly coupled to the neighboring ones. The narrow saturation hole in the absorber causes the inverted Lamb dip.

The authors in Refs. 11 and 12 are able to explain the qualitative features of the experiments, but they are clearly aware of the limitations of perturbation theory if quantitative features are desired. In addition hysteresis effects cannot be understood within third-order perturbation theory, and already the fifth-order results are considerably involved. Beterov, Lisitsyn, and Chebotaev<sup>4,5</sup> solve the problem within the approximation usually referred to as the REA (rate-equation approximation; see, e.g., Ref. 13). They derive the analytic expressions for the case when the inhomogeneous linewidth greatly exceeds the homogeneous one (the Doppler limit). This gives simple results when there is exact resonance between the atomic transition and the cavity mode and also when these are detuned by a considerable amount. Greenstein<sup>14</sup> presents a discussion, which

is essentially equivalent to the REA, even if differently formulated.

In this paper<sup>15</sup> we shall present a calculational method based on the continued fraction approach of Stenholm and Lamb.<sup>16</sup> This is exact for one-mode operation of any intensity. Its lowest approximation is the REA, which here is evaluated without the use of the Doppler limit. We also give a brief discussion of the influence of a simple collision model on our results within the REA.

In Sec. II we derive the equations of motion for the cavity modes and the components of the atomic polarization. These are given for a multimode case more general than is needed for this paper; in subsequent publications we will use these results to discuss other features of the system. In Sec. III we construct the steady-state characteristics of the system in the REA. Section IV investigates the accuracy of this approximation and its corrections. Finally, Sec. V briefly considers the inclusion of collision effects.

## II. GENERAL THEORY

### A. Model of the System

The theoretical model to be used consists of two mirrors forming the optical cavity, into which the absorption and amplification cells are inserted. The technical details of the experiment, e.g., the cavity losses and the pumping of the cells, are incorporated into the phenomenological parameters of the model. The electromagnetic field is linearly polarized by Brewster windows in the cells, and we assume it to oscillate in longitudinal modes only, neglecting the transverse variation of the mode intensities.

In accordance with the semiclassical theory of Lamb<sup>17</sup> we assume the field in the cavity to be described by Maxwell's equations. The inhomogeneous driving term in the wave equation is the induced atomic polarization, which in turn is calculated from the preassigned field. This way the electromagnetic field is determined self-consistently by the saturation properties of the nonlinear medium.

The linear losses of the cavity modes are determined by their phenomenological quality factors  $Q_n$  giving the width  $\Omega_n/Q_n$ , which normally is much smaller than the separation between the longitudinal modes. The driving polarization can thus be written as a discrete sum over components oscillating with nearly the cavity eigenfrequencies. Each driving component induces a field oscillating at the same frequency owing to the linearity of the wave equation. The coupling between the modes takes place in the nonlinear medium.

As there is no spatial overlap between the am-

plifying and absorbing regions we can separate the polarization into two components,

$$P(z, t) = P^{\text{amp}}(z, t) + P^{\text{abs}}(z, t), \quad (2.1)$$

and no cross processes occur. From this we immediately deduce that the two terms in the polarization can be calculated independently, each one from its own cell. The different driving components of  $P$  can most easily be separated according to their spatial behavior. Following Lamb<sup>17</sup> we introduce the projection

$$\begin{aligned} & \frac{2}{L} \int_0^L dz \sin(K_n z) P(z, t) \\ &= \frac{2}{L_{\text{amp}}} \int_0^{L_{\text{amp}}} dz \sin(K_n z) \frac{L_{\text{amp}}}{L} P^{\text{amp}}(z, t) \\ &+ \frac{2}{L_{\text{abs}}} \int_0^{L_{\text{abs}}} dz \sin(K_n z) \frac{L_{\text{abs}}}{L} P^{\text{abs}}(z, t), \quad (2.2) \end{aligned}$$

which acts as the driving term of the cavity mode  $n$ . In (2.2),  $L$  is the length of the cavity, and  $L_{\text{amp}}$  and  $L_{\text{abs}}$  are the lengths of the cells. We notice that the filling factors  $L_{\text{amp}}/L$  and  $L_{\text{abs}}/L$  will multiply the contributions to the polarization component. These factors can, however, be absorbed into the phenomenological parameters characterizing the pumping rates in the two cells and need no explicit consideration.

Lee *et al.*<sup>1</sup> remark that the lengths and positions of the cells are of some importance for the proper working of the laser system. This is easily understood on account of the dispersion in the active media and the standing wave variation of the field. The calculation in (2.2) involves a certain choice of positions of the cells but these end effects will not be discussed subsequently.

The amplifying medium is assumed to consist of a set of two-level atoms with the following characteristics: The energy difference is  $E_a - E_b = \hbar\omega$ ; the levels decay with the rates  $\gamma_a$  and  $\gamma_b$ , respectively, and they are populated by the pumping mechanism at the rates  $\lambda_a$  and  $\lambda_b$ ; the levels are coupled by the dipole matrix element  $\wp$ . The atomic parameters  $\omega$ ,  $\gamma_a$ , and  $\gamma_b$  are taken to be pressure dependent. The time development of this system is described by a  $2 \times 2$  density matrix, which we calculate assuming the electric field to remain fixed. Having obtained the solution, we determine the induced polarization. This adiabatic procedure is justified because the intensities of the modes change at the rate  $\Omega_n/Q_n$ , which usually is at least an order of magnitude less than the rate of change of the atomic state determined by the decay rates  $\gamma_a$  and  $\gamma_b$ . The atomic transitions are Doppler broadened by the assumedly Gaussian velocity distribution of width  $Ku$ . The dimensionless intensity of mode

$n$  in the amplifier cell is chosen as (see Lamb<sup>17</sup>)

$$I_n = \frac{\varphi^2 |E_n|^2}{2\hbar^2 \gamma_a \gamma_b}. \quad (2.3)$$

We assume that the absorbing gas can be described with a model similar to the amplifying medium, but with different values of the characterizing parameters. The absorber linewidths  $\gamma_a^{\text{abs}}$  and  $\gamma_b^{\text{abs}}$  are chosen different from those in the amplifier by keeping the cells at different pressures or using different gases in the absorption and amplification cells. By keeping the amplifier cell at a higher pressure than the absorption cell, one can broaden the amplifier linewidths more which, however, causes the resonance frequencies of the media to be shifted. In case we have different gases in the cells, the dipole matrix elements and level spacings are unequal. In this work we assume the resonance frequencies to be the same in both cells. A generalization of the present treatment is trivially carried out to relax this restriction.

The dimensionless intensity of mode  $n$  in the absorber cell is written

$$I_n^{\text{abs}} = \alpha I_n, \quad (2.4)$$

$$\alpha = \frac{\gamma_a \gamma_b}{\gamma_a^{\text{abs}} \gamma_b^{\text{abs}}} \left( \frac{\varphi^{\text{abs}}}{\varphi} \right)^2. \quad (2.5)$$

In the following we shall assume that  $\alpha$  is larger than 1, which implies that the absorber saturates more easily than the amplifier.<sup>18</sup>

In Secs. II B–II C we develop the basic equations of motion for this model in a form which will prove useful for the present investigation.

### B. Electromagnetic Field Equations

In accordance with the theory of Lamb we choose the cavity eigenfunctions  $\sin(K_n z)$  with the corresponding eigenfrequencies  $\Omega_n = K_n c$ . In order to eliminate the rapidly varying components from the field amplitudes, we separate the mode frequencies expanding the field as follows:

$$E(z, t) = \sum_n \frac{1}{2} [E_n(t) e^{-i\Omega_n t} + E_n^*(t) e^{i\Omega_n t}] \sin(K_n z). \quad (2.6)$$

The slowly varying amplitudes  $E_n(t)$  are generally complex, in contradistinction to the field amplitudes used by Lamb.<sup>17</sup> The active medium shifts the oscillational frequency to the position

$$\nu_n = \Omega_n - \frac{d}{dt} \arg E_n(t) \Big|_{t=(\text{const})}. \quad (2.7)$$

The shifts are different in the two cells, but in the following we shall neglect that. In a manner similar to (2.6), we write the polarization as

$$P(z, t) = \sum_n \frac{1}{2} [P_n(t) e^{-i\Omega_n t} + P_n^*(t) e^{i\Omega_n t}] \sin(K_n z). \quad (2.8)$$

From Maxwell's equations we obtain (see, e.g., Stenholm<sup>13</sup>) the relation

$$\left( \frac{\partial^2}{\partial t^2} + \frac{1}{\tau_n} \frac{\partial}{\partial t} - c^2 \frac{\partial^2}{\partial z^2} \right) E(z, t) = -\frac{1}{\epsilon_0} \frac{\partial^2}{\partial t^2} P(z, t), \quad (2.9)$$

where  $Q_n = \Omega_n \tau_n$  is the quality factor of the cavity mode  $n$ . Introducing the expressions (2.6) and (2.8) into (2.9) and neglecting the supposedly small terms  $\ddot{E}_n$ ,  $\dot{E}_n/\tau_n$ ,  $\ddot{P}_n$ , and  $\Omega_n \dot{P}_n$ , we obtain

$$\left( \frac{\partial}{\partial t} + \frac{1}{2\tau_n} \right) E_n(t) = \frac{i\Omega_n}{2\epsilon_0} P_n(t), \quad (2.10)$$

which describes the time evolution of the slowly varying part of the amplitude of the cavity mode  $n$  under the action of the driving field  $P_n(t)$ .

It proves convenient to introduce the complex nonlinear susceptibilities formally<sup>19</sup> by

$$\chi_n(E_1, \dots, E_N) = P_n(E_1, \dots, E_N) / \epsilon_0 E_n. \quad (2.11)$$

With this definition Eq. (2.10) separates into

$$\left( \frac{\partial}{\partial t} + \frac{1}{2\tau_n} \right) |E_n| = -\frac{Q_n}{2\tau_n} (\text{Im } \chi_n) |E_n|, \quad (2.12)$$

$$\frac{\partial}{\partial t} \arg E_n = \frac{Q_n}{2\tau_n} (\text{Re } \chi_n). \quad (2.13)$$

Equation (2.13) describes the dispersion in the active medium and hence the shift (2.7) of the oscillational frequency. It turns out that Eq. (2.12), which determines the amplification (attenuation) of the mode, is not very sensitive to small frequency shifts, and therefore we shall ignore the difference between  $\nu_n$  and  $\Omega_n$  in the following and proceed to consider Eq. (2.12) only. Instead of the magnitude, it is more convenient to employ the dimensionless intensity  $I_n$  defined by (2.3) for which (2.12) gives the equation

$$\begin{aligned} \frac{\partial I_n}{\partial t} &= -\frac{1}{\tau_n} [Q_n (\text{Im } \chi_n) + 1] I_n \\ &\equiv \frac{1}{\tau_n} H_n(I_1, \dots, I_N) I_n. \end{aligned} \quad (2.14)$$

Clearly the gain functions  $H_n$  depend also on the frequencies of the modes, but this is not displayed. The set of equations (2.14) determines the field amplitudes once we know the gain functions  $H_n$ .

Recalling the additivity of the amplitudes of polarization in the two cells [cf. Eq. (2.2)], we can write

$$H_n = G_n^{\text{amp}} - G_n^{\text{abs}} - 1, \quad (2.15)$$

$$G_n^{\text{amp, abs}} = Q_n |\text{Im } \chi_n^{\text{amp, abs}}|, \quad (2.16)$$

where we have explicitly included the correct signs of the contributions. According to the adiabatic procedure the functions  $H_n$  can be calculated from given intensities  $I_n$ . Determining new values of  $I_n$  from (2.14) and recalculating the gain functions  $H_n$ , we obtain the temporal behavior of the mode intensities. Steady state is achieved when the right-hand side of (2.14) vanishes.

### C. Polarization of the Medium

The set of two-level atoms constituting the active medium is described by the density matrix  $\rho$ . Instead of the diagonal components we prefer to use the combinations  $N = \rho_{aa} - \rho_{bb}$  and  $M = \rho_{aa} + \rho_{bb}$  (see Stenholm and Lamb<sup>16</sup>), which are related by the equation

$$M(z, v, t) = (\lambda_a + \lambda_b)/\gamma - \frac{1}{2}(\gamma_a - \gamma_b) \times \int_{-\infty}^t dt' e^{-\gamma(t-t')} N(z, v, t'). \quad (2.17)$$

Equation (2.17) enables us to eliminate  $M$  and write an equation for  $N$  only

$$\left(\frac{d}{dt} + \gamma\right) N(z, v, t) - \frac{1}{4}(\gamma_a - \gamma_b)^2 \times \int_{-\infty}^t dt' e^{-\gamma(t-t')} N(z, v, t') = + \frac{\lambda_a \gamma_b - \lambda_b \gamma_a}{\gamma} - \frac{2i\varphi}{\hbar} E(z(t), t) \times [\rho_{ab}(z, v, t) - \rho_{ba}(z, v, t)], \quad (2.18)$$

with  $\gamma = \frac{1}{2}(\gamma_a + \gamma_b)$  being the transverse relaxation rate. The time dependence of  $z$  is taken to be

$$z(t) = z - v(t_f - t), \quad (2.19)$$

where  $t_f$  is the final time for which the polarization is desired<sup>20</sup> at the point  $z$ . The off-diagonal elements obey the equation of motion

$$\left(\frac{d}{dt} + \gamma + i\omega\right) \rho_{ab}(z, v, t) = -\frac{i\varphi}{\hbar} E(z(t), t) N(z, v, t) \quad (2.20)$$

and its complex conjugate for  $\rho_{ba}$ .

The assumed electromagnetic field is now written

$$E(z(t), t) = \sum_{K, \nu} E(K, \nu) e^{i[Kz(t) - \nu t]}, \quad (2.21)$$

where  $K$  and  $\nu$  go over the cavity-mode wave vectors  $K_n$  and eigenfrequencies  $\Omega_n$  and their combinations.<sup>21</sup> A comparison of (2.6) with (2.21) yields

$$E(K, \nu) = \frac{1}{4i} \sum_{n=1}^N (E_n \delta_{\nu, \Omega_n} + E_n^* \delta_{\nu, -\Omega_n}) \Delta(K, K_n), \quad (2.22)$$

$$\Delta(K, K_n) = \delta_{K, K_n} - \delta_{K, -K_n}. \quad (2.23)$$

A natural ansatz to solve Eqs. (2.18) and (2.20) is the Fourier series

$$\rho_{ab}(z, v, t) = \sum_{K, \nu} \rho_{ab}(K, \nu, v) e^{i[Kz(t) - \nu t]}, \quad (2.24)$$

$$N(z, v, t) = \sum_{K, \nu} N(K, \nu, v) e^{i[Kz(t) - \nu t]}. \quad (2.25)$$

Inserting (2.21), (2.24), and (2.25) into (2.18) and (2.20) and identifying the corresponding Fourier coefficients on both sides, we obtain the coupled difference equations

$$\rho_{ab}(K, \nu) = -\frac{i\varphi}{\gamma\hbar} \mathcal{L}(\omega - \nu + K\nu) \times \sum_{K', \nu'} E(K', \nu') N(K - K', \nu - \nu'), \quad (2.26)$$

$$\rho_{ba}(K, \nu) = \frac{i\varphi}{\gamma\hbar} \mathcal{L}(\omega + \nu - K\nu)^* \times \sum_{K', \nu'} E(K', \nu') N(K - K', \nu - \nu'), \quad (2.27)$$

$$N(K, \nu) L(K, \nu) - \lambda(K, \nu) = -\frac{2i\varphi\gamma}{\hbar\gamma_a\gamma_b} \sum_{K', \nu'} E(K', \nu') \times [\rho_{ab}(K - K', \nu - \nu') - \rho_{ba}(K - K', \nu - \nu')], \quad (2.28)$$

where

$$\mathcal{L}(x) = \gamma/(\gamma + ix), \quad (2.29)$$

$$L(K, \nu) = \frac{\gamma}{\gamma_a\gamma_b} \left( \gamma - i\nu + iK\nu - \frac{\frac{1}{4}(\gamma_a - \gamma_b)^2}{\gamma - i\nu + iK\nu} \right), \quad (2.30)$$

$$\lambda(K, \nu) = \left( \frac{\lambda_a}{\gamma_a} - \frac{\lambda_b}{\gamma_b} \right) \delta_{K,0} \delta_{\nu,0} \equiv \lambda \delta_{K,0} \delta_{\nu,0}. \quad (2.31)$$

For simplicity we assume the pumping term  $\lambda$  independent of  $z$ ,  $t$ , and  $\nu$  in each cell.

The complex Lorentzian (2.29) becomes negligible once  $|x| \gg \gamma$  which fact enables us to perform a rotating-wave approximation in Eqs. (2.26)–(2.28). Because of the Lorentzian in front of the sum in (2.26),  $\rho_{ab}(K, \nu)$  has non-negligible values only near the point  $\nu = \omega$  in a region of width  $Ku$ . Similarly, the influential components of  $\rho_{ba}(K, \nu)$  are located in the vicinity of  $\nu = -\omega$ . Dividing (2.28) by  $L(K, \nu)$ , we notice that  $N(K, \nu)$  becomes negligible unless  $\nu$  is small (of the order  $Ku$ ).

Introducing  $E(K, \nu)$  from (2.22) and performing

the rotating-wave approximation, we find

$$\begin{aligned} \rho_{ab}(K, \nu) = & -\frac{\wp}{4\gamma\hbar} \mathcal{L}(\omega - \nu + K\nu) \\ & \times \sum_{K', p} E_p \Delta(K', K_p) N(K - K', \nu - \Omega_p), \end{aligned} \quad (2.32)$$

$$\begin{aligned} \rho_{ba}(K, \nu) = & \frac{\wp}{4\gamma\hbar} \mathcal{L}(\omega + \nu - K\nu)^* \\ & \times \sum_{K', p} E_p^* \Delta(K', K_p) N(K - K', \nu + \Omega_p), \end{aligned} \quad (2.33)$$

where  $p$  goes from 1 to  $N$  ( $N$  is the number of modes involved), and in (2.32)  $\nu$  is taken to be near  $\omega$  and in (2.33) near  $-\omega$ . Inserting these expressions into (2.28) and interchanging  $n$ ,  $p$  and  $K'$ ,  $K''$  in the part coming from  $\rho_{ba}$ , we obtain the recursion relation for the Fourier coefficients of the population inversion

$$\begin{aligned} N(K, \nu) L(K, \nu) - \lambda(K, \nu) \\ = \frac{1}{4} \sum_{K', K'', p, n} I_{pn} \Delta(K', K_n) \Delta(K'', K_p) \\ \times [\mathcal{L}(\omega - \nu - \Omega_n + K\nu - K'\nu) \\ + \mathcal{L}(\omega + \nu - \Omega_p - K\nu + K''\nu)^*] \\ \times N(K - K' - K'', \nu + \Omega_n - \Omega_p), \end{aligned} \quad (2.34)$$

where we have defined analogously with (2.3)

$$I_{pn} = \wp^2 E_p E_n^* / 2\hbar^2 \gamma_a \gamma_b, \quad (2.35)$$

from which  $I_{nn} = I_n$ .

The problem is to solve the difference equation (2.34) letting the indices  $n$  and  $p$  run over the number of modes involved. Some symmetry properties of the solutions, which will be needed in the following, are listed in Appendix A.

The atomic polarization is obtained from the solution by averaging over the velocity distribution  $W(v)$

$$\begin{aligned} P(z, t) = c_0 \wp \int_{-\infty}^{+\infty} dv W(v) \\ \times [\rho_{ab}(z, \nu, t) + \rho_{ba}(z, \nu, t)], \end{aligned} \quad (2.36)$$

where the density of active atoms  $c_0$  has been introduced because of the normalization of the density matrix. Inserting (2.24) and its complex conjugate into (2.36), we find

$$\begin{aligned} P(z, t) = c_0 \wp \sum_{K, \nu} \left( \int_{-\infty}^{+\infty} dv W(v) \right. \\ \left. \times [\rho_{ab}(K, \nu, v) + \rho_{ba}(K, \nu, v)] \right) \\ \times e^{i(Kz - \nu t)}. \end{aligned} \quad (2.37)$$

Comparing this with the expansion (2.8), we obtain

$$\begin{aligned} (1/4i)P_n(t) = c_0 \wp \int_{-\infty}^{+\infty} dv W(v) \rho_{ab}(K_n, \Omega_n, v) \\ = -c_0 \wp \int_{-\infty}^{+\infty} dv W(v) \rho_{ba}(-K_n, \Omega_n, -v), \end{aligned} \quad (2.38)$$

where the properties  $W(-v) = W(v)$  and (A4) have been utilized. The coefficients  $\rho_{ab}(K, \nu, v)$  are calculated by (2.32), and we find

$$\begin{aligned} P_n = -\frac{ic_0 \wp^2}{\gamma\hbar} \int_{-\infty}^{+\infty} dv W(v) \mathcal{L}(\omega - \Omega_n + K_n v) \\ \times \sum_{K', p} E_p \Delta(K', K_p) N(K_n - K', \Omega_n - \Omega_p, v). \end{aligned} \quad (2.39)$$

From the derived expression we can easily extract the complex nonlinear susceptibility (2.11). According to (2.14) its imaginary part determines the amplification factor  $G_n$  of the cell, and we find with the aid of (2.16)

$$\begin{aligned} G_n = \frac{c_0 \wp^2 Q_n}{\epsilon_0 \gamma \hbar} \int_{-\infty}^{+\infty} dv W(v) \operatorname{Re} \left( \mathcal{L}(\omega - \Omega_n + K_n v) \right. \\ \left. \times \sum_{K', p} \frac{E_p}{E_n} \Delta(K', K_p) N(K_n - K', \Omega_n - \Omega_p, v) \right). \end{aligned} \quad (2.40)$$

The expression is valid for either cell, provided that we use the appropriate values of the atomic parameters, and it automatically produces the correct sign—positive if there is population inversion in the material and negative otherwise.

At this point it ought to be pointed out that a study of the dynamics of the laser should include an integration of (2.40) over the radial distribution of the beam. Here, however, we neglect this on account of the additional complexity arising (see Beterov *et al.*<sup>4,5</sup>). In steady state the present treatment is correct provided that the intensities refer to areas over which the transverse variation is small and self-focusing can be neglected.

#### D. Exact Solution for One Mode

When only one mode is oscillating the difference equations derived in Sec. IIC can be solved exactly. The solution is the same as the one obtained by Stenholm and Lamb<sup>16</sup> in the form of a continued fraction (CFS). The new aspect of this work is the inclusion of the absorption cell into the optical cavity.

In the one-mode case the sums over  $p$  and  $n$  in (2.34) contain the term  $p = n = 1$  only. The frequency variables of the Fourier coefficients become equal on both sides, and because only the

component  $\lambda(K, 0)$  differs from zero, we must take  $\nu = 0$ . The sums over  $K'$  and  $K''$  can be carried out utilizing (2.23). As the inhomogeneous term  $\lambda(K, 0)$  vanishes unless  $K = 0$  only the values  $K = rK_1$  with  $r = 0, \pm 2, \pm 4, \dots$ , occur. Introducing the new unknowns

$$n_r = N(rK_1, 0)/\lambda, \quad (2.41)$$

we obtain from (2.34) the three-term recurrence relation

$$A_r n_r - B_{r-1} n_{r-2} - B_{r+1} n_{r+2} = \delta_{r,0}, \quad (2.42)$$

where

$$A_r = L(rK, 0) + B_{r-1} + B_{r+1} \quad (2.43)$$

$$B_r = \frac{1}{4} I [\mathcal{L}(\omega - \Omega + rKv) + \mathcal{L}(\omega - \Omega - rKv)^*], \quad (2.44)$$

and the subscript 1 on  $K_1$ ,  $\Omega_1$ , and  $I_1$  has been omitted as unnecessary.

For  $r \neq 0$  we can solve the ratio of successive  $n_r$  from (2.42) and find

$$C_r = \frac{n_r}{n_{r-2}} = \frac{B_{r-1}}{A_r - B_{r+1} n_{r+2}/n_r} = \frac{B_{r-1}}{A_r - B_{r+1}^2 / (A_{r+2} - \dots)}, \quad r > 0 \quad (2.45)$$

$$D_r = \frac{n_r}{n_{r+2}} = \frac{B_{r+1}}{A_r - B_{r-1} n_{r-2}/n_r} = \frac{B_{r+1}}{A_r - B_{r-1}^2 / (A_{r-2} - \dots)}, \quad r < 0. \quad (2.46)$$

Setting  $r = 2$  in (2.45),  $r = -2$  in (2.46), and inserting these into the equation (2.42) with  $r = 0$ , we obtain

$$n_0 = [A_0 - B_{-1} D_{-2} - B_1 C_2]^{-1} = [A_0 - 2 \operatorname{Re}(B_1 C_2)]^{-1}, \quad (2.47)$$

where the properties of  $A_r$  and  $B_r$  have been used to write  $(B_{-1} D_{-2}) = (B_1 C_2)^*$  [this property is also immediately verified from Eq. (A1)].

The amplification factor (2.40) for the single oscillating mode is

$$G = \frac{c_0 \varphi^2 Q}{\epsilon_0 \gamma \hbar} \int_{-\infty}^{+\infty} dv W(v) \times \operatorname{Re} \{ \mathcal{L}(\omega - \Omega + Kv) [N(0, 0, v) - N(2K, 0, v)] \}. \quad (2.48)$$

The calculated  $n_r$  determine the nonzero coefficients  $N(K, 0)$  by (2.41), and from the relations (2.47) and (2.45) with  $r = 2$  we obtain

$$G = \frac{\bar{N} \varphi^2 Q}{\epsilon_0 \gamma \hbar} \int_{-\infty}^{+\infty} dv W(v) \frac{\operatorname{Re} [\mathcal{L}(\omega - \Omega + Kv)(1 - C_2)]}{A_0 - 2 \operatorname{Re}(B_1 C_2)}, \quad (2.49)$$

where  $\bar{N} = c_0 \lambda$ . This is the exact CFS result which can be used for both the amplifier and the absorber.

Even though the continued fraction in (2.49) generally converges quite rapidly, the numerical calculation of the integral over  $v$  is time consuming. Consequently a simpler approximate solution is presented in Sec. II E.

#### E. REA Solution

The rate-equation approximation consists of setting  $C_2 = D_{-2} = 0$ . Then we obtain from (2.49) and (2.43)

$$G = \frac{\bar{N} \varphi^2 Q}{\epsilon_0 \gamma \hbar} \int_{-\infty}^{+\infty} dv W(v) \times \frac{\mathcal{L}_r(\omega - \Omega + Kv)}{1 + \frac{1}{2} I [\mathcal{L}_r(\omega - \Omega + Kv) + \mathcal{L}_r(\omega - \Omega - Kv)]}, \quad (2.50)$$

where

$$\mathcal{L}_r(x) = \operatorname{Re} \mathcal{L}(x) = \gamma^2 / (\gamma^2 + x^2). \quad (2.51)$$

Expanding the integrand into partial fractions we can express the result in terms of the plasma dispersion function  $Z$  as follows:

$$G = \frac{2 \varphi^2 \bar{N} Q}{\epsilon_0 \hbar K u} \left[ A_1 Z\left(\frac{\gamma x_1}{K u}\right) + A_3 Z\left(\frac{\gamma x_3}{K u}\right) \right]. \quad (2.52)$$

The expressions for  $A_1$ ,  $A_3$ ,  $x_1$ , and  $x_3$  and the details of the derivation are given in Appendix C. Some of the properties of the plasma dispersion function are discussed in Appendix B.

When the oscillating mode is tuned to exact resonance with the atomic transition we obtain from the results of Appendix C that

$$G = \frac{\varphi^2 \bar{N} Q}{\epsilon_0 \hbar K u} \frac{Z_1(i \kappa (1 + I)^{1/2})}{(1 + I)^{1/2}}, \quad (2.53)$$

and for detunings far off resonance, i.e.,  $|\omega - \Omega| \gg \gamma$ , we have

$$G = \frac{\varphi^2 \bar{N} Q}{\epsilon_0 \hbar K u} \frac{Z_1((\Omega - \omega)/K u + i \kappa (1 + \frac{1}{2} I)^{1/2})}{(1 + \frac{1}{2} I)^{1/2}}, \quad (2.54)$$

where  $\kappa = \gamma / K u$  is the Doppler parameter. The situation described by (2.54) is equivalent with that of two oppositely traveling noninteracting waves each of amplitude  $\frac{1}{2} E$ .

The use of the REA to obtain numerical results rests on the fact that the plasma dispersion function can be easily programmed on the computer and the time consuming velocity integration is avoided. In addition, the derivatives with respect to the intensity and the detuning, which we shall need in the following, are relatively simple (see Appendix C). We shall return to the question

of the accuracy and applicability of the REA in Sec. IV.

### III. ONE-MODE BEHAVIOR IN THE REA

#### A. General Features of the System

We first consider the behavior of the system in the REA. This gives the total gain at zero intensity correctly. Assuming the absorption cell turned off, we obtain from (2.15) and (2.52)

$$H = \frac{\varphi^2 Q \bar{N}}{\epsilon_0 \hbar K u} Z_i(\Delta + i\kappa) - 1, \quad (3.1)$$

which agrees with (2.49) for  $I=0$ . The detuning parameter for both cells is

$$\Delta = (\Omega - \omega)/Ku. \quad (3.2)$$

The imaginary part of the plasma dispersion function reaches its maximum at  $\Omega = \omega$ , and therefore, when  $H=0$ , the threshold pumping value  $\bar{N}_{\text{TR}}$  is obtained from (3.1) at exact resonant tuning  $\Delta=0$ . We define the relative excitation by

$$\mathfrak{X} = \frac{\bar{N}}{\bar{N}_{\text{TR}}} = \frac{\varphi^2 Q \bar{N}}{\epsilon_0 \hbar K u} Z_i(i\kappa). \quad (3.3)$$

The contribution of the amplifier cell to the total gain is now written as

$$G^{\text{amp}} = \mathfrak{X}g(\Delta, \kappa, I), \quad (3.4)$$

where the exact normalized amplification factor  $g_{\text{amp}}$  is, by (2.49),

$$g(\Delta, \kappa, I) = \frac{1}{\kappa Z_i(i\kappa)} \int_{-\infty}^{+\infty} dv W(v) \times \frac{\text{Re}[\mathcal{L}(\omega - \Omega + Kv)(1 - C_2)]}{A_0 - 2\text{Re}(B_1 C_2)}. \quad (3.5)$$

In the REA the corresponding expression is, according to (2.52),

$$g = \frac{2}{Z_i(i\kappa)} [A_1 Z(\kappa x_1) + A_3 Z(\kappa x_3)]. \quad (3.6)$$

The linewidth in the absorber cell is

$$\gamma^{\text{abs}} = \zeta\gamma, \quad (3.7)$$

where we assume  $\zeta < 1$ . It is convenient to normalize the absorber cell pumping rate analogously with (3.3):

$$\mathfrak{M} = (\varphi^{\text{abs}})^2 Q |\bar{N}^{\text{abs}}| Z_i(i\zeta\kappa) / \epsilon_0 \hbar K u, \quad (3.8)$$

where we explicitly take into account the minus sign in (2.15). It should be noted that the value  $\mathfrak{M}=1$  is not connected with any specific threshold in the laser but is chosen merely as an expedient dimensionless reference point. For simplicity we have assumed the same kinetic temperature for both gases in the cells ( $u \propto T^{1/2}$ ). In the numerical

work we choose  $\gamma_a = \gamma_b = \gamma$ , which is easily relaxed in calculations on specific laser systems.<sup>22</sup>

The total gain function (2.15) is now

$$H = \mathfrak{X}g(\Delta, \kappa, I) - \mathfrak{M}g(\Delta, \zeta\kappa, \alpha I) - 1. \quad (3.9)$$

We assume that the parameters  $\mathfrak{X}$  and  $\mathfrak{M}$  can be chosen arbitrarily by pumping the two cells independently. All changes in  $\kappa$ ,  $\zeta$ , and  $\alpha$  due to changes in pumping currents are ignored.

The steady-state solutions of the equation (2.14) are determined by

$$H(\Delta, I_\infty)I_\infty = 0, \quad (3.10)$$

which is satisfied if either  $H=0$  or  $I_\infty=0$ . In the following we restrict our consideration to the stable solutions  $I_\infty$  only. If  $I_\infty \neq 0$ , the linearized equation (2.14)

$$\delta \dot{I} = \frac{I_\infty}{\tau} \left( \frac{\partial H}{\partial I} \right)_{I_\infty} \delta I \quad (3.11)$$

must have an exponentially decaying solution, which requires that

$$\left( \frac{\partial H}{\partial I} \right)_{I_\infty} < 0. \quad (3.12)$$

The nonoscillating solution  $I_\infty=0$  is stable provided that

$$H(\Delta, 0) < 0, \quad (3.13)$$

independent of the sign of the derivative. For resonant tuning  $\Delta=0$ , we obtain from (3.6) [cf. also Eq. (2.53)]

$$g(0, \kappa, I) = \frac{1}{(1+I)^{1/2}} \frac{Z_i(i\kappa(1+I)^{1/2})}{Z_i(i\kappa)}. \quad (3.14)$$

For small values of  $\kappa$  and reasonable intensities (i.e.,  $\kappa I^{1/2} \ll 1$ ) the ratio of the imaginary parts of the plasma dispersion functions equals approximately 1, and from (3.9) we find

$$H(0, I) = \frac{\mathfrak{X}}{(1+I)^{1/2}} - \frac{\mathfrak{M}}{(1+\alpha I)^{1/2}} - 1. \quad (3.15)$$

With no absorption ( $\mathfrak{M}=0$ ),  $H$  decreases monotonously as  $I$  increases, and as soon as  $\mathfrak{X} > 1$  we have one and only one stable solution of (3.10). For  $\mathfrak{M} \neq 0$  the function  $H(0, I)$  may acquire a maximum (recall that  $\alpha > 1$ ). The occurrence of nonmonotonic gain was first discussed by Kazantsev *et al.*<sup>12</sup> in the framework of fifth-order perturbation theory.

These general features can be verified in the full REA expressions. Calculated results are displayed in Fig. 1. Depending on the amount of absorption for fixed amplifier cell pumping  $\mathfrak{X}$  and detuning  $\Delta$ , three different regions are observed: (a)  $H(\Delta, 0) > 0$  gives only one stable solution; (b)  $H(\Delta, 0) < 0$ , but  $\max[H(\Delta, I)] > 0$  gives two stable

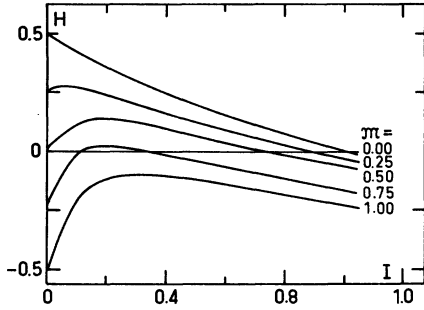


FIG. 1. Gain function  $H$  at exact resonance versus the intensity  $I$  for various pumping rates. The state of the amplifier is kept fixed ( $\mathfrak{N}=1.5$ ,  $\kappa=0.1$ , and  $\zeta=0.25$ ).

operating points—one at  $I=0$  and the other at the zero of  $H(\Delta, I)$  where  $\partial H/\partial I < 0$ ; (c)  $\text{Max}[H(\Delta, I)] < 0$  gives again only one stable solution  $I=0$ . In the region where (b) is valid the operation is bistable. It turns out to be informative to represent the conditions for bistability as regions in the  $(\mathfrak{N}, \mathfrak{M})$  plane. The detailed construction of these diagrams is discussed in Sec. III B. Figure 2 shows an example for resonant tuning. In region II we have two stable operating points: Increasing the amount of absorption we reach the region I where the oscillation is extinguished, or decreasing  $\mathfrak{M}$  leads to region III with a unique nonzero solution.

From Figs. 1 and 2 it is clear that hysteresis effects are observed when  $\mathfrak{N}$  or  $\mathfrak{M}$  is varied over a closed cycle passing through the bistable region. Two examples<sup>23</sup> of this are shown in Figs. 3 and 4. Similar hysteresis effects occur when we keep the operating point  $(\mathfrak{N}, \mathfrak{M})$  fixed but detune the laser system (Fig. 5). The origin of this behavior is evident from the results of Sec. III B. The existence of these hysteresis effects was verified experimentally by Lee *et al.*<sup>1</sup> and Lisitzyn *et al.*<sup>3</sup> but they tried to avoid the bistable region.

We have assumed that  $\zeta$  was roughly 0.3 in the experiment performed by Lee *et al.*<sup>1</sup> and estimate that  $\mathfrak{N}$  was below 1.3, which is suggested by the

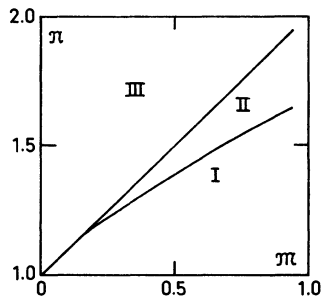


FIG. 2. Regions of different behavior in single-mode operation. The parameters as in Fig. 1.

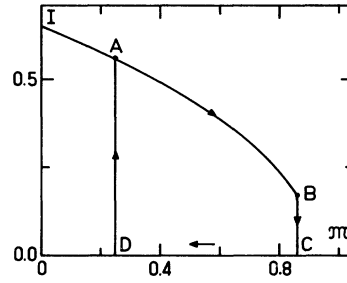


FIG. 3. Current hysteresis for a modulation of the absorber cell pumping  $\mathfrak{M}$ . Increasing  $\mathfrak{M}$  ( $\mathfrak{N}=1.3$ ) decreases the steady-state intensity  $I$  until at point  $B$  the stable solution coincides with the unstable one and oscillation ceases. It begins to grow from noise only at point  $D$ . The region  $A \rightarrow B$  or  $C \rightarrow D$  corresponds to the bistable solution. In this figure  $\omega = \Omega$ ,  $\kappa = 0.025$ , and  $\zeta = 0.1$ .

value for the tuning range obtained from (3.1). Then Fig. 2 shows that bistable operation occurs for values of  $\mathfrak{M}$  larger than 90% of the value required to extinguish the oscillation completely. This is in agreement with the experimental estimate given in Ref. 1.

B. Calculation of the Operating Characteristics

For fixed detuning  $(\Omega - \omega) = \Delta Ku$  and for fixed  $\zeta$  (i.e., the pressures in the cells are kept constant) the operating conditions are determined solely by the two pumping parameters  $\mathfrak{N}$  and  $\mathfrak{M}$ , and hence we display the steady state characteristics in the  $(\mathfrak{M}, \mathfrak{N})$  plane as explained previously.

From Fig. 1 it is clear that the region for one stable nonzero solution is determined by the relation

$$H(\Delta, 0) = \mathfrak{N}g(\Delta, \kappa, 0) - \mathfrak{M}g(\Delta, \zeta, \kappa, 0) - 1 \geq 0, \tag{3.16}$$

where the curve corresponding to the equality sign is a straight line in the  $(\mathfrak{M}, \mathfrak{N})$  plane above which the inequality holds. Below the line the

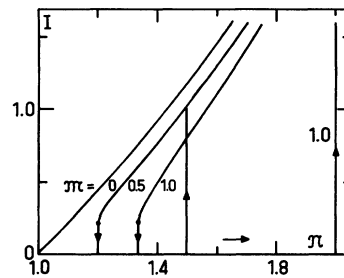


FIG. 4. Same as Fig. 3 but the amplifier cell pumping is modulated with  $\mathfrak{M}$  fixed.

system may have either two stable solutions or the single nonoscillating solution  $I=0$ . The border between these two types of behavior arises when the maximum of the total gain  $H(\Delta, I)$  occurs at the amplification threshold  $H(\Delta, I)=0$ . From Fig. 1 we see that this situation takes place when the loss line is tangential to the gain curve, and consequently the two equations

$$\mathfrak{N}g(\Delta, \kappa, I) - \mathfrak{M}g(\Delta, \zeta\kappa, \alpha I) - 1 = 0, \quad (3.17)$$

$$\mathfrak{N} \frac{\partial g(\Delta, \kappa, I)}{\partial I} - \mathfrak{M} \frac{\partial g(\Delta, \zeta\kappa, \alpha I)}{\partial I} = 0 \quad (3.18)$$

must be satisfied simultaneously. Solving these for  $\mathfrak{N}$  and  $\mathfrak{M}$  as functions of  $I$ , we get a parametric representation of a curve in the  $(\mathfrak{M}, \mathfrak{N})$  plane. Below this curve the oscillation is extinguished ( $I=0$ ), and above it up to the line (3.16) we obtain bistable behavior. The curve meets the line (3.16) at the point where (3.18) is valid for  $I=0$  which merely indicates, that a minimum amount of absorption is needed to give a maximum in the gain for non-negative values of  $I$ , implying the possibility of bistable operation. From (C8) and (C18)–(C21) it follows that in the Doppler limit ( $\kappa \ll 1$ )

$$\left. \frac{\partial g(\Delta, \kappa, I)}{\partial I} \right|_{I=0} = - \frac{Z_i(\Delta + i\kappa)}{4Z_i(i\kappa)} \left[ 1 + \left( 1 + \frac{\Delta^2}{\kappa^2} \right)^{-1} \right]. \quad (3.19)$$

Introducing (3.19) with appropriate values of the arguments into (3.18) and utilizing (3.16) to eliminate  $\mathfrak{N}$ , we obtain for the minimum absorption required to achieve bistable operation the value

$$\mathfrak{M} = \left( \alpha \frac{1 + \gamma^2/[\gamma^2 + \alpha(\Omega - \omega)^2]}{1 + \gamma^2/[\gamma^2 + (\Omega - \omega)^2]} - 1 \right)^{-1} \frac{Z_i(i\zeta\kappa)}{Z_i(\Delta + i\zeta\kappa)}, \quad (3.20)$$

which for resonant tuning reduces to  $(\alpha - 1)^{-1}$ . This gives a very small value of  $\mathfrak{M}$  for large  $\alpha$ . Figures 6 and 7 show some calculated curves,

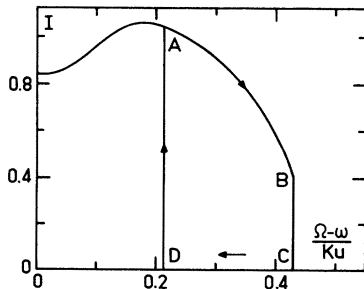


FIG. 5. Frequency hysteresis when  $\mathfrak{N}=1.6$ ,  $\mathfrak{M}=0.56$ ,  $\kappa=0.1$ , and  $\zeta=0.25$ . At B the oscillation is suddenly cut off and is restarted only if the detuning is diminished to D.

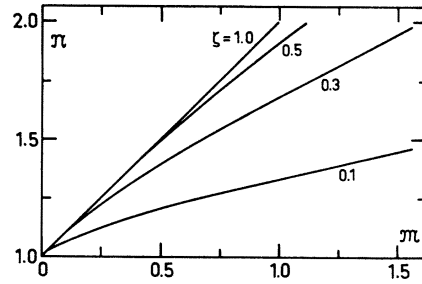


FIG. 6. Size of the bistable region for various  $\zeta$  at exactly resonant tuning ( $\kappa=0.025$ ).

that divide the  $(\mathfrak{M}, \mathfrak{N})$  plane into regions of different steady-state behavior. In Fig. 6 the size of the bistable region is considered as a function of the ratio  $\zeta = \gamma^{\text{abs}}/\gamma$ . For  $\zeta=1$  both cells saturate identically [ $H = (\mathfrak{N} - \mathfrak{M})g - 1$ ], and hence the bistable region disappears. For  $\zeta < 1$  ( $\alpha > 1$ ) the absorber saturates more strongly, and the region of bistable operation grows with decreasing  $\zeta$ . In Fig. 7 we have plotted the bistable regions for various detunings keeping  $\zeta$  fixed. The inclination to bistability is found to be most prominent near resonant tuning where the active medium saturates most strongly and hence the contrast between the saturation states of the cells is enhanced.

The previous discussion explained what solution to expect when we know the pumping parameters  $\mathfrak{N}$  and  $\mathfrak{M}$ . For fixed values of these the equation

$$H = \mathfrak{N}g(\Delta, \kappa, I) - \mathfrak{M}g(\Delta, \zeta\kappa, \alpha I) - 1 = 0 \quad (3.21)$$

has to be solved to give the intensity  $I$ . A general explicit solution is not possible even in the REA. A straightforward way of treating (3.21) is to plot  $H(\Delta, I)$  and from its zero obtain  $I_\infty$  (cf. Fig. 1). More general information is made available if we draw the straight lines (3.21) in the  $(\mathfrak{M}, \mathfrak{N})$  plane regarding  $I$  as a parameter. A set of such lines is shown in Fig. 8 together with the region of bistable operation. Within the bistable region one stable solution is always  $I=0$ , and the second value of  $I$  satisfying (3.21) corresponds to the unstable operating point and will hence be omitted.

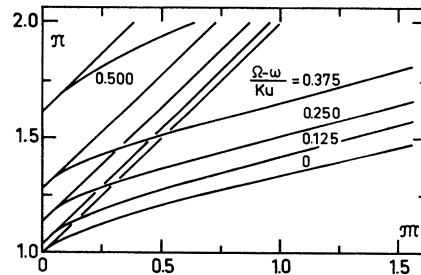


FIG. 7. Bistable region for various detunings ( $\kappa=0.025$  and  $\zeta=0.1$ ).

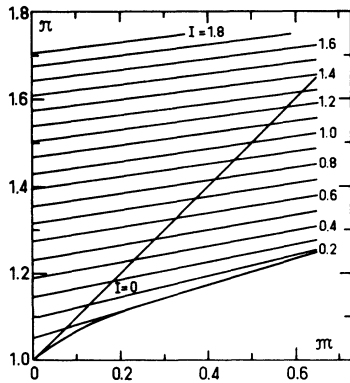


FIG. 8. Steady-state intensity at exact resonance with  $\kappa = 0.025$  and  $\zeta = 0.1$ . The borders of bistable operation are also included. Below the line  $I = 0$  one stable solution is always  $I = 0$ .

The line (3.21) with constant  $I$  is tangential to the border line of the nonoscillatory region at the point where (3.18) is simultaneously satisfied. After the point of contact the fixed  $I$  value does, however, belong to the unstable solution as can be seen from Fig. 9, and consequently the lines (3.21) are to be drawn only to the point of contact.

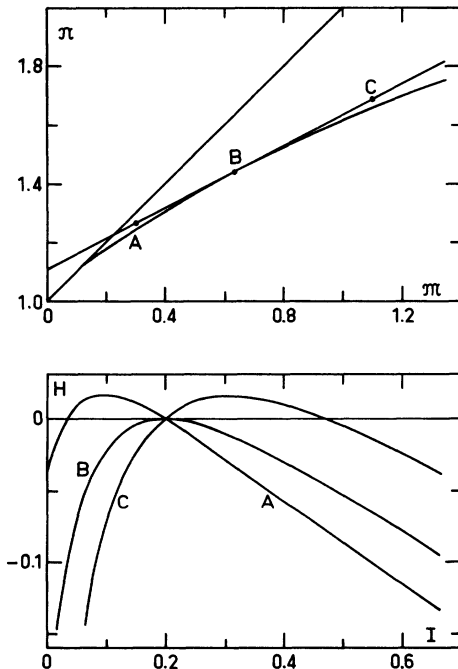


FIG. 9. Construction of Fig. 8. The point A corresponds to the pumping rates  $(\mathcal{M}, \mathcal{N}) = (0.30, 1.26)$ , B to  $(0.63, 1.44)$ , and C to  $(1.10, 1.68)$ . The corresponding gain functions are displayed in the lower picture. The intensity  $I$  equals 0.2, and other parameters are as in Fig. 8.

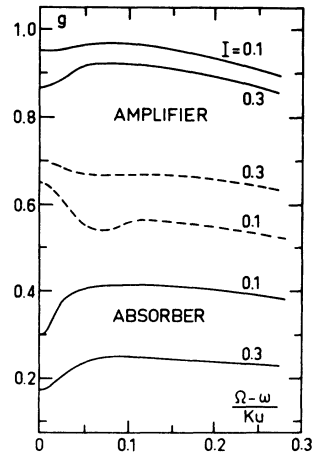


FIG. 10. Normalized gain factors of the amplifier and the absorber cells with  $\kappa = 0.025$  and  $\zeta = 0.1$ . To facilitate the comparison of the dips, we have also drawn their difference (dashed lines).

C. Detuning Curves

The experimental results are often presented in the form of detuning curves, i.e., the steady-state intensity is plotted versus detuning  $\Omega - \omega$ . The Lamb dip and the inverted Lamb dip appear in these curves. The occurrence of the inverted Lamb dip can be explained already in the framework of third-order perturbation theory (Lisitsyn and Chebotaev<sup>2</sup>). The different saturation state in the absorber and amplifier cell give rise to a peak in the total amplification at resonant tuning causing an inverted Lamb dip for sufficiently large absorption (see Fig. 10).

In order to obtain the detuning curves we use equation (3.21) to plot  $\mathcal{M}$  as a function of  $I$  with

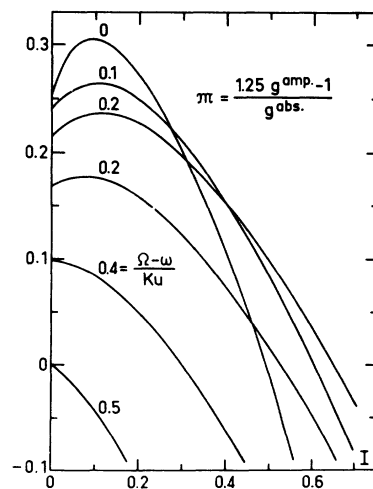


FIG. 11. Curves needed to construct Fig. 12.

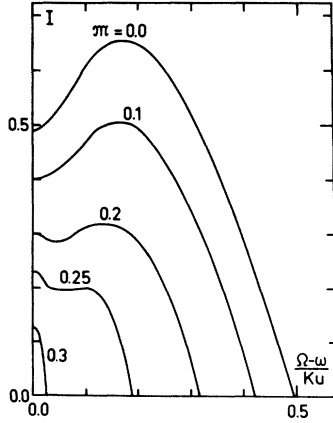


FIG. 12. Detuning curves with  $\mathfrak{N}=1.25$ ,  $\kappa=0.1$ , and  $\xi=0.25$ . The curves are symmetric with respect to the ordinate axis.

$\Delta = (\Omega - \omega)/Ku$  as a parameter and  $\mathfrak{N}$  fixed. An example is shown in Fig. 11. We construct the detuning curves by drawing a line of constant  $\mathfrak{N}$  and plotting the corresponding values of  $I$  versus  $\Delta$ . In Fig. 12 the results obtained from Fig. 11 are shown, and we see how starting from  $\mathfrak{N}=0$  with an ordinary Lamb dip of width  $\gamma$  an increasing  $\mathfrak{N}$  leads to the inverted Lamb dip of width  $\gamma_{\text{abs}} = \xi\gamma$ . The dips are, of course, distorted by power broadening which affects the amplifier less than the more easily saturable absorber.

Greenstein<sup>14</sup> has discussed the inverted Lamb dip in some detail but it appears to be useful to give an analytic formula for its occurrence. From Fig. 12 we see that the ordinary Lamb dip goes over into an inverted Lamb dip when the second derivative of  $I$  with respect to  $\Delta$  changes its sign at  $\Delta=0$ . This guarantees only the existence of an inverted Lamb dip but not the disappearance of the ordinary Lamb dip, as can be verified from Fig. 12. We expand the implicit equation (3.21) near  $\Delta=0$ :

$$H(0, I) + \left( \frac{\partial H}{\partial \Delta} + \frac{\partial H}{\partial I} \frac{\partial I}{\partial \Delta} \right) \Delta + \frac{1}{2} \left[ \frac{\partial^2 H}{\partial \Delta^2} + 2 \frac{\partial^2 H}{\partial \Delta \partial I} \frac{\partial I}{\partial \Delta} + \frac{\partial^2 H}{\partial I^2} \left( \frac{\partial I}{\partial \Delta} \right)^2 + \left( \frac{\partial H}{\partial I} \right) \frac{\partial^2 I}{\partial \Delta^2} \right] \Delta^2 + \dots = 0. \quad (3.22)$$

For the steady-state value of  $I$  we have  $H(0, I_\infty) = 0$  and

$$\left. \frac{\partial H}{\partial \Delta} \right|_{\Delta=0} = 0, \quad \left. \frac{\partial I_\infty}{\partial \Delta} \right|_{\Delta=0} = 0 \quad (3.23)$$

for symmetry reasons. Thus the condition that the second derivative of  $I$  vanishes gives the relation

$$\begin{aligned} \frac{\partial^2 I}{\partial \Delta^2} &= \left( -\frac{\partial H}{\partial I} \right)^{-1} \frac{\partial^2 H}{\partial \Delta^2} \\ &= \left( -\frac{\partial H}{\partial I} \right)^{-1} \left( \mathfrak{N} \frac{\partial^2 g}{\partial \Delta^2} - \mathfrak{N} \frac{\partial^2 g}{\partial \Delta^2} \right) = 0. \end{aligned} \quad (3.24)$$

At the stable operating point we have  $\partial H/\partial I < 0$ , and it follows that  $\partial^2 I/\partial \Delta^2$  has the same sign as  $\partial^2 H/\partial \Delta^2$ . From (C15) and (3.24) we obtain

$$-\mathfrak{N}f(\kappa, I) + \frac{1}{\alpha} \mathfrak{N}f(\xi\kappa, \alpha I) = 0, \quad (3.25)$$

$$\begin{aligned} f(\kappa, I) &= 1 - \frac{Z_i(i\kappa(1+I)^{1/2})}{Z_i(i\kappa)} \frac{1 + \frac{3}{2}I + \frac{3}{8}I^2}{(1+I)^{3/2}} \\ &\quad - \frac{\kappa I(1 + \frac{3}{4}I)}{(1+I)Z_i(i\kappa)} \left[ 1 - \kappa(1+I)^{1/2} Z_i(i\kappa(1+I)^{1/2}) \right], \end{aligned} \quad (3.26)$$

which together with the equation

$$H = \frac{\mathfrak{N}Z_i(i\kappa(1+I)^{1/2})}{(1+I)^{1/2}Z_i(i\kappa)} - \frac{\mathfrak{N}Z_i(i\xi\kappa(1+\alpha I)^{1/2})}{(1+\alpha I)^{1/2}Z_i(i\xi\kappa)} - 1 = 0 \quad (3.27)$$

determines the minimum value of  $\mathfrak{N}$  needed to obtain an inverted Lamb dip. In the extreme Doppler limit  $\kappa=0$  the condition reduces to

$$\begin{aligned} \mathfrak{N} &\geq (1+\alpha I)^{1/2} \left( \alpha^2 \frac{1+I}{1+\alpha I} \frac{8+9\alpha I}{8+9I} \right. \\ &\quad \left. \times \frac{8+12I+3I^2+8(1+I)^{3/2}}{8+12\alpha I+3\alpha^2 I^2+8(1+\alpha I)^{3/2}} - 1 \right)^{-1}, \end{aligned} \quad (3.28)$$

where we have chosen  $I$  as the independent variable and the corresponding value of  $\mathfrak{N}$  is to be determined from (3.27). For  $I=0$  the relation (3.28) gives  $\mathfrak{N} \geq (\alpha^2 - 1)^{-1}$ . If we take a nonzero value for  $\kappa$  we obtain for small values of  $I$  the relation

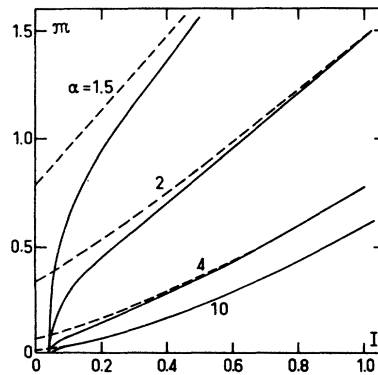


FIG. 13. For given intensity this figure gives the minimum absorption needed to obtain an inverted Lamb dip for the Doppler parameters  $\kappa=0.1$  (solid line) and  $\kappa=0$  (dashed line).

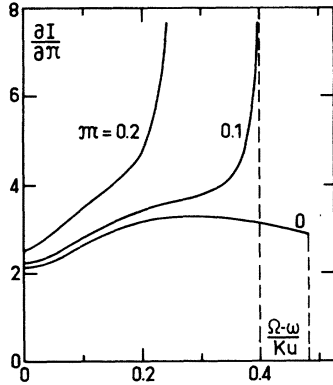


FIG. 14. Dynamic response of the laser system to the modulation of the amplifier cell pumping ( $\mathfrak{N}=1.25$ ,  $\kappa=0.1$ , and  $\zeta=0.25$ ).

$$\mathfrak{N} \geq \left( \frac{\alpha^2 I - 4\kappa^2}{I - 4\kappa^2} - 1 \right)^{-1} \quad (3.29)$$

from which it follows that we must have  $I \geq 4\kappa^2$  in order to get a positive value for  $\mathfrak{N}$ .<sup>24</sup> Some numerical results are shown in Fig. 13.

#### D. Dynamic Characteristics

Bolwijn *et al.*<sup>25</sup> have shown that there may be a more pronounced structure in the ac response of a laser system than in the ordinary dc response. Stenholm and Lamb<sup>16</sup> show that this holds only for a limited range of intensities. It is of some interest to see how the presence of the absorber affects the dynamic response.

For a sufficiently slow modulation of the pumping or the loss parameters we can use the linearized form of Eq. (2.14) to obtain the response

$$\delta I = \left. \frac{\partial I}{\partial \mathfrak{N}} \right|_{\mathfrak{N}_0} \delta \mathfrak{N}, \quad (3.30)$$

and similarly for the modulation of  $\mathfrak{K}$ . From (3.21) we find directly

$$\frac{\partial I}{\partial \mathfrak{N}} = g^{\text{abs}} \left( \frac{\partial H}{\partial I} \right)^{-1}, \quad (3.31)$$

$$\frac{\partial I}{\partial \mathfrak{K}} = -g^{\text{amp}} \left( \frac{\partial H}{\partial I} \right)^{-1}, \quad (3.32)$$

because  $H$  disappears at the operating point, which is stable if  $\partial H / \partial I < 0$ . The response of the amplifier exceeds the response of the absorber, because, for a fixed  $I$ ,  $g^{\text{amp}} > g^{\text{abs}}$ , but it is of interest to consider the modulation of the absorber cell pumping as this is a new degree of freedom in the system. The derivatives in (3.31) and (3.32) are directly determined by the slopes in Fig. 11 with  $\mathfrak{N}$  fixed. In the REA one can use (C18)–(C21) to get explicit results. Numerical results are shown

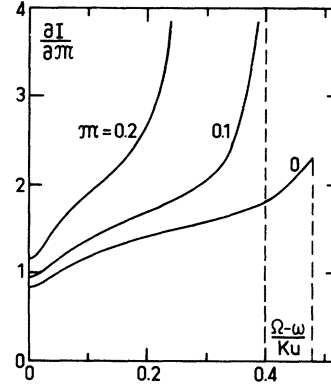


FIG. 15. Same as Fig. 14 except that the absorption is modulated.

in Figs. 14 and 15.

In the region of bistable operation the enhancement factor  $(\partial H / \partial I)^{-1}$  in (3.31) and (3.32) becomes large, and at the border between bistable and nonoscillating regions it diverges. For  $\mathfrak{N}=0$  the curve  $\partial I / \partial \mathfrak{N}$  reproduces the result of Ref. 16, but we notice that the curve for  $\partial I / \partial \mathfrak{N}$  at  $\mathfrak{N}=0$  has a quite different shape. For the values of  $\mathfrak{N}$  leading to bistable operation a singularity develops at the edge of the amplifying range. Here, of course, the linearization implied in (3.30) breaks down.

It is also seen from Figs. 14 and 15 that the central dip in  $\partial I / \partial \mathfrak{N}$  has approximately the width  $\gamma$  and the dip in  $\partial I / \partial \mathfrak{K}$  has the width  $\zeta\gamma$ , which in certain ranges of the parameters  $\mathfrak{N}$  and  $\mathfrak{K}$  could be used to measure the two linewidths with better accuracy than the dc curves of Fig. 12 admit. In this paper we shall, however, not try to determine the optimum range of the parameters for such experiments.

## IV. EXACT RESULTS FOR ONE MODE

### A. Validity of the REA

In this section we shall give numerical results for the exact normalized gain factor  $g(\Delta, \kappa, I)$  and compare these to the REA results. Qualitatively the REA reproduces all the features of the laser system correctly, and therefore we shall not repeat the calculations presented in the previous part. In Sec. IV B we briefly discuss where the REA should be replaced by exact results when higher accuracy is required.

We now show that the REA coincides with the exact results for small values of  $I$  in the Doppler limit and for a very large value of  $I$ . For small  $I$ , the third-order expansion of (2.49) and (2.52) gives

$$g - g_{\text{REA}} = -\frac{I}{(1+4a^2)Z_i(i\kappa)} \left( \frac{Z_i(\frac{1}{2}i\kappa) - Z_i - 2aZ_r}{1+4a^2} + \frac{Z_r}{4a} - \frac{\kappa}{2} [1 + \kappa a Z_r - \kappa Z_i - 2\kappa a^2 Z_i - 2\kappa a Z_r] \right) + O(I^2), \quad (4.1)$$

where  $a = (\Omega - \omega)/\gamma$ . The function  $Z = Z_r + iZ_i$  is to be evaluated with the argument  $(a+i)\kappa$  unless otherwise is explicitly indicated. The difference (4.1) is obviously large only near  $a=0$  because of the factor  $(1+4a^2)^{-1}$  on the right-hand side. In the Doppler limit  $Z_i \approx \pi^{1/2}$  and  $Z_r/a$  is of the order  $\kappa$  [see Eq. (B6)], and therefore (4.1) vanishes at least as  $\kappa$ .

For very large values of  $I$  we must use the asymptotic expression of  $Z$  [Eq. (B7)] and, from (3.14) we obtain at resonant tuning

$$g(0, \kappa, I) = [\kappa Z_i(i\kappa)I]^{-1} + O(I^{-2}), \quad (4.2)$$

which is in agreement with the exact asymptotic behavior derived by Stenholm.<sup>26</sup> If one does not use the correct asymptotic expression for  $Z$ , namely, one ignores the fact that power broadening makes the Doppler-limit approximation invalid, the incorrect asymptotic behavior  $g \propto I^{-1/2}$  results.

Utilizing the properties of  $B_r$  and  $A_r$  and the recurrence relation (2.42) with  $r=0$ , one can show that the integrand in (2.48) is

$$\text{Re}[\mathcal{L}(\omega - \Omega + K\nu)(n_0 - n_2)]$$

$$= \frac{1 - n_0}{I} = \frac{2 \text{Re} B_1}{IA_0} + \frac{2 \text{Re}(B_1 C_2 n_0)}{IA_0}. \quad (4.3)$$

From the first equation we note that the exact gain factor is proportional to the area of the holes

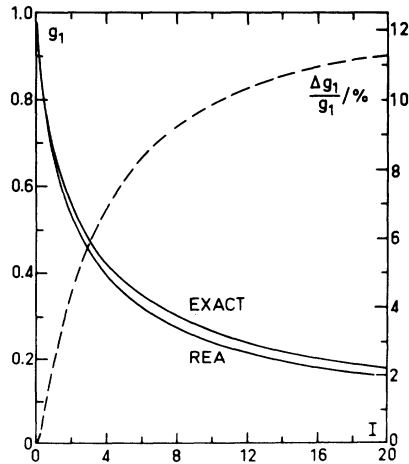


FIG. 16. Normalized gain factor at exact resonance with  $\kappa=0.1$ . The relative error in the REA is given by the dashed line (the relative error on the right-hand scale).

burned into the velocity distribution (cf. Bennett<sup>27</sup>). The first term in the second equation is the REA contribution. If the CFS solution converges,  $C_2$  approaches a finite constant as  $I$  increases, and for physical reasons we can, on the other hand, conclude that  $n_0$  approaches zero, and hence, for very large values of  $I$ , we can ignore the second term compared to the first one.

We have compared the exact results to those of the REA numerically in Figs. 16 and 17. The exact curves are calculated truncating the computation of the continued fraction of  $C_2$  when for a fixed value of  $\nu$  the next estimate differs less than  $10^{-6}$  from the previous one (for a convenient algorithm calculating continued fractions, see Feldman and Feld<sup>28</sup>). The integration over  $\nu$  is carried out with Simpson's formula using the step length  $K\nu/\gamma=0.1$  near the origin and near the maximum of the Lorentzian. We use larger step lengths when going away from these regions. The point where the integration can be halted is estimated from the remainder of the integrated gain factor

$$\delta g \approx \exp \left[ -\kappa^2 \left( \frac{K\nu}{\gamma} \right)^2 \right] / \left[ \pi \kappa^2 \left( \frac{K\nu}{\gamma} \right)^3 \right], \quad (4.4)$$

which can easily be derived from (3.5). The approximate overall error in  $g$  is less than 0.2%.

From Fig. 17 we see that the worst case occurs near resonant tuning. This is easily understood on account of the results by Stenholm and Lamb,<sup>16</sup> who show that the velocity distribution exhibits

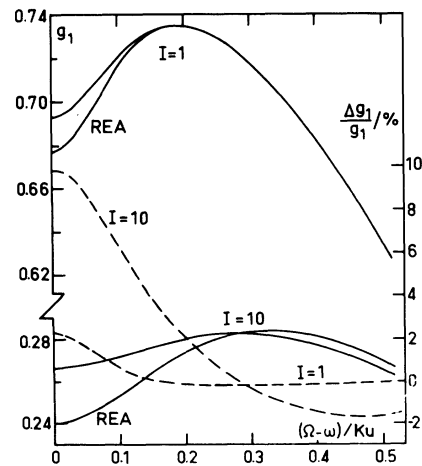


FIG. 17. Normalized gain factors for various detunings with  $I=1$  and  $10$  ( $\kappa=0.1$ ). The corresponding relative errors are given by the dashed lines (scale on the right).

ripples near the origin which are absent in the REA. One fact to be noted is that the REA over-emphasizes the Lamb dip because of its incapability to reproduce this structure. From Fig. 16 we see that with realistic values of  $I$ , i.e.,  $I \lesssim 1$ , the REA introduces an error that is less than 2%. In most applications this is sufficiently accurate.

#### B. Discussion of the REA

The main advantage of the REA is that we avoid the velocity integration as we already stated. This becomes especially important when we need the derivatives of  $g$  with respect to  $I$  or the detuning. In the exact method several values of  $g$  must be calculated near the point where the derivative is to be evaluated if good accuracy in numerical calculations is needed.

In certain regions the errors tend to cancel when we calculate  $H$  because a change  $\Delta H$  is composed of two contributions, i.e.,

$$\Delta H = \mathfrak{X} \Delta g^{\text{amp}} - \mathfrak{M} \Delta g^{\text{abs}}. \quad (4.5)$$

This cancellation is rather efficient because  $\mathfrak{X} > \mathfrak{M}$  and normally  $\Delta g^{\text{amp}}$  is of the same sign but smaller than  $\Delta g^{\text{abs}}$ . The error may be large when one computes properties that depend on the position of the maximum of  $H$ . If, however, the intensity acts only as phenomenological label of the curves, the REA may still produce reasonably good results (cf. the construction of the lower limit of the bistable region). We do not give any numerical comparison here.

Comparing to the other major approximations in this work, i.e., taking the pressure effects into account by a Lorentzian broadening mechanism, neglecting the radial distribution of the field and ignoring the focusing, we consider the use of the REA to be justified in most cases.

#### V. INCLUSION OF PRESSURE EFFECTS

When the atoms of the whole velocity profile sustain single-mode oscillation in the laser, the details of the atomic collision processes are presumably averaged out. The effects of increased pressure can then be discussed within a simple parametrization of atomic collision events, and their influence on the present calculations will be briefly considered. We have previously discussed a model<sup>29</sup> where both velocity and phase changing collisions are included but the correlation between these processes is neglected. The resulting gain factor is

$$G = \frac{\wp^2 \bar{N} Q}{\epsilon_0 \gamma \hbar} \varphi(\bar{I}, \Delta) \left( 1 + \bar{I} \frac{\gamma_0^2 T}{\gamma(1 + \gamma_0 T)} \varphi(\bar{I}, \Delta) \right)^{-1}, \quad (5.1)$$

where

$$\bar{N} = c_0(\lambda_a - \lambda_0)/\gamma_0, \quad (5.2)$$

$$\gamma = \gamma_0 + (1/T)(1 - \cos\eta), \quad (5.3)$$

$$\Delta = \omega - \Omega + (1/T)\sin\eta, \quad (5.4)$$

$$\bar{I} = \wp^2 |E|^2 / 2\hbar^2 \gamma_0^2, \quad (5.5)$$

$$\mathfrak{L}_r(x) = \gamma^2 / (\gamma^2 + x^2), \quad (5.6)$$

$$\begin{aligned} \varphi(\bar{I}, \Delta) = & \int_{-\infty}^{+\infty} dv W(v) \frac{1}{2} [\mathfrak{L}_r(\Delta + Kv) + \mathfrak{L}_r(\Delta - Kv)] \\ & \times \left( 1 + \frac{1}{2} \bar{I} \frac{\gamma_0^2 T}{\gamma(1 + \gamma_0 T)} [\mathfrak{L}_r(\Delta + Kv) \right. \\ & \left. + \mathfrak{L}_r(\Delta - Kv)] \right)^{-1} \end{aligned} \quad (5.7)$$

In (5.1)–(5.7),  $\gamma_0$  is the free atom and  $\gamma$  the pressure-broadened linewidth,  $T$  is the average time between collisions, and  $\eta$  the average phase change in a collision. Comparing (5.7) with (C1) we find

$$\begin{aligned} G = & \frac{\gamma}{\gamma_0} G_{\text{REA}} \left( \Delta, \frac{\gamma}{Ku}, \frac{\gamma T}{1 + \gamma_0 T} I \right) \\ & \times \left[ 1 + I \frac{\gamma T}{1 + \gamma_0 T} \frac{\gamma \epsilon_0 \hbar}{\wp^2 \bar{N} Q} \right. \\ & \left. \times G_{\text{REA}} \left( \Delta, \frac{\gamma}{Ku}, \frac{\gamma T}{1 + \gamma_0 T} I \right) \right]^{-1}, \end{aligned} \quad (5.8)$$

where  $I$  is the dimensionless intensity defined by (2.3). Introducing the normalized gain factor  $g$  we obtain

$$G = \frac{\gamma}{\gamma_0} \mathfrak{X} g \left( 1 + I \frac{\gamma T}{1 + \gamma_0 T} \kappa Z_i(i\kappa) \mathfrak{X} g \right)^{-1}, \quad (5.9)$$

where  $g$  is calculated with the arguments  $\Delta$ ,  $\kappa$ ,  $[\gamma T / (1 + \gamma_0 T)] I$ . In the Doppler limit we can neglect the second term in the denominator, and consequently

$$G = (\gamma/\gamma_0) \mathfrak{X} g(\Delta, \kappa, \xi I), \quad (5.10)$$

where

$$\xi = \frac{\gamma_0 T}{1 + \gamma_0 T} \frac{\gamma}{\gamma_0}. \quad (5.11)$$

Because  $\mathfrak{X}$  is a free parameter we can include  $\gamma/\gamma_0$  into it, and we conclude that in the Doppler limit we are allowed to use the REA results with  $\xi$  given by (5.11) and the pressure shift of the resonant frequency included into  $\Delta$ .

#### APPENDIX A: SYMMETRY PROPERTIES OF THE FOURIER COEFFICIENTS

Taking the complex conjugate of (2.25), changing the summation indices  $K, \nu$  to  $-K, -\nu$  and recalling

that  $N(z, t, v)$  must be real, we find

$$N(-K, -\nu, v) = N(K, \nu, v)^*. \quad (\text{A1})$$

Applying the same procedure to (2.24) and recalling that  $\rho_{ab} = (\rho_{ba})^*$ , we obtain

$$\rho_{ab}(-K, -\nu, v) = \rho_{ba}(K, \nu, v)^*. \quad (\text{A2})$$

Replacing  $K$  by  $-K$ ,  $v$  by  $-v$ , and changing  $K'$  to  $-K'$  and  $K''$  to  $-K''$  in (2.34) and remembering that  $\Delta(-K, K_n) = -\Delta(K, K_n)$ , we see that  $N(-K, \nu, -v)$  satisfies the same equation as  $N(K, \nu, v)$  [note that  $\lambda(-K, \nu, -v) = \lambda(K, \nu, v)$ ] and consequently

$$N(-K, \nu, -v) = N(K, \nu, v). \quad (\text{A3})$$

From (2.32) we obtain by (A3) that

$$\rho_{ab}(-K, \nu, -v) = -\rho_{ab}(K, \nu, v), \quad (\text{A4})$$

and from (2.33)

$$\rho_{ba}(-K, \nu, -v) = -\rho_{ba}(K, \nu, v). \quad (\text{A5})$$

#### APPENDIX B: PLASMA DISPERSION FUNCTION

The plasma dispersion function is defined by

$$Z(\zeta) = \frac{1}{\pi^{1/2}} \int_{-\infty}^{+\infty} \frac{dt e^{-t^2}}{t - \zeta} \equiv Z_r(\zeta) + i Z_i(\zeta), \quad (\text{B1})$$

where  $\zeta = x + iy$  and  $y > 0$ . From the symmetry relations

$$Z_r(\zeta) = Z_r(x, y) = -Z_r(-x, y), \quad (\text{B2})$$

$$Z_i(\zeta) = Z_i(x, y) = Z_i(-x, y), \quad (\text{B3})$$

it follows that in the present context we have for  $y < 0$

$$Z(\zeta^*) = [Z(\zeta)]^* = -[Z(-\zeta)]^* \quad (\text{B4})$$

instead of the ordinary expression (see, e.g., Fried and Conte<sup>30</sup> or Abramovitz and Stegun<sup>31</sup>)

$$Z(\zeta^*) = Z(\zeta) + 2i\pi^{1/2} e^{-\zeta^2}. \quad (\text{B5})$$

For small values of  $\zeta$  we have

$$Z(\zeta) = i\pi^{1/2} e^{-\zeta^2} - 2\zeta(1 - \frac{2}{3}\zeta^2 + \frac{3}{4}\zeta^4 + \dots), \quad (\text{B6})$$

and for large values of  $\zeta$

$$Z(\zeta) = -\frac{1}{\zeta} \left( 1 + \frac{1}{2\zeta^2} + \frac{3}{4\zeta^4} + \dots \right) \quad (\text{Im}\zeta > 0). \quad (\text{B7})$$

In the whole complex plane the derivative of  $Z$  is

$$\frac{dZ}{d\zeta} = -2(1 + \zeta Z). \quad (\text{B8})$$

From (B1)–(B8) it can be shown that

$$\int_{-\infty}^{+\infty} dv W(v) \mathcal{L}(\omega - \Omega \pm Kv) = -\frac{i\gamma}{Ku} Z(\zeta), \quad (\text{B9})$$

$$\int_{-\infty}^{+\infty} dv W(v) \mathcal{L}(\omega - \Omega \pm Kv)^* = \frac{i\gamma}{Ku} [Z(\zeta)]^*, \quad (\text{B10})$$

$$\begin{aligned} \int_{-\infty}^{+\infty} dv W(v) [\mathcal{L}(\omega - \Omega + Kv)]^k \\ = \frac{1}{(k-1)!} \left( -\frac{i\gamma}{Ku} \right)^k \frac{\partial^{k-1}}{\partial \zeta^{k-1}} Z(\zeta), \end{aligned} \quad (\text{B11})$$

where

$$\zeta = (\Omega - \omega)/Ku + i\gamma/Ku, \quad (\text{B12})$$

$$W(v) = (1/\pi^{1/2}u) e^{-v^2/u^2}, \quad (\text{B13})$$

$$\mathcal{L}(x) = \gamma/(\gamma + ix). \quad (\text{B14})$$

#### APPENDIX C: REA

Symmetrizing the integrand with respect to  $v$  in formula (2.50) and using (3.3) and (3.4), we obtain

$$\begin{aligned} g = \frac{1}{\kappa Z_i(i\kappa)} \int_{-\infty}^{+\infty} dv W(v) \\ \times \frac{1}{2} [\mathcal{L}_r(\omega - \Omega + Kv) + \mathcal{L}_r(\omega - \Omega - Kv)] \\ \times \{ 1 + \frac{1}{2} I [\mathcal{L}_r(\omega - \Omega + Kv) + \mathcal{L}_r(\omega - \Omega - Kv)] \}^{-1}, \end{aligned} \quad (\text{C1})$$

which is written as

$$g = \frac{1}{\kappa Z_i(i\kappa)} \int_{-\infty}^{+\infty} dv W(v) f\left(\frac{\Omega - \omega}{\gamma}, I, \frac{Kv}{\gamma}\right), \quad (\text{C2})$$

$$\begin{aligned} f(a, I, x) = (1 + a^2 + x^2) [(1 + a^2 + x^2)^2 \\ - 4a^2x^2 + I(1 + a^2 + x^2)]^{-1}. \end{aligned} \quad (\text{C3})$$

The function  $f(a, I, x)$  can be expanded as

$$f(a, I, x) = \sum_{i=1}^4 A_i(a, I) [x - x_i(a, I)]^{-1} \quad (\text{C4})$$

if the roots of the denominator in (C3), i.e.,

$$\begin{aligned} x_i = \pm [a^2 - 1 - \frac{1}{2}I \pm (\frac{1}{4}I^2 - 4a^2 - 2a^2I)^{1/2}]^{1/2} \\ \equiv \pm (c \pm d)^{1/2} \end{aligned} \quad (\text{C5})$$

do not coincide. Fourfold roots do not exist because  $c^2 > d^2$ , and double roots cause no trouble because they can be treated with a proper limiting process. If we label the roots  $x_1 = -x_2 = (c + d)^{1/2}$  and  $x_3 = -x_4 = (c - d)^{1/2}$ , we obtain

$$A_1 = -A_2 = (1 + a^2 + x_1^2)/4dx_1, \quad (\text{C6})$$

$$A_3 = -A_4 = -(1 + a^2 + x_3^2)/4dx_3. \quad (\text{C7})$$

Introducing the expansion (C4) into (C1) and carrying out the integration over  $v$  with the aid of (B1) and utilizing the properties  $x_1 = -x_2$ ,  $x_3 = -x_4$ ,  $A_1 = -A_2$ ,  $A_3 = -A_4$ , and the formulas (B2) and (B3),

we get

$$g = \frac{2}{Z_i(i\kappa)} [A_1 Z(\kappa x_1) + A_3 Z(\kappa x_3)]. \quad (\text{C8})$$

For values  $a^2 \ll I$  we derive from (C5)–(C7) the expansions

$$x_1 = i \left( 1 + \frac{a^2}{2I} (4+I) \right) + O(a^4), \quad (\text{C9})$$

$$x_3 = i(1+I)^{1/2} \left( 1 - \frac{a^2}{2I} \frac{4+3I}{1+I} \right) + O(a^4), \quad (\text{C10})$$

$$A_1 = \frac{2ia^2}{I^2} + O(a^4), \quad (\text{C11})$$

$$g = \frac{1}{Z_i(i\kappa)} \left[ \frac{Z_i(i\kappa(1+I)^{1/2})}{(1+I)^{1/2}} - \frac{4a^2}{I^2} \left( Z_i(i\kappa) - Z_i(i\kappa(1+I)^{1/2}) \frac{1 + \frac{3}{2}I + \frac{3}{8}I^2}{(1+I)^{3/2}} - \frac{\kappa I (1 + \frac{3}{4}I)}{1+I} [1 - \kappa(1+I)^{1/2} Z_i(i\kappa(1+I)^{1/2})] \right) \right], \quad (\text{C15})$$

which at resonant tuning  $a=0$  gives (2.53). For very large detunings  $a^2 \gg 1+I$  we obtain from (C5)–(C7)

$$x_1 = x_3^* = a + i(1 + \frac{1}{2}I)^{1/2}, \quad (\text{C16})$$

$$A_1 = A_3^* = [4i(1 + \frac{1}{2}I)^{1/2}]^{-1}. \quad (\text{C17})$$

Insertion of these into (C8) gives (2.54).

For the determination of the bistable region we need the derivative of (C8) with respect to the intensity  $I$ . From (C5)–(C7) and (B8) a straightforward calculation gives the results

$$A_3 = \frac{1}{2i(1+I)^{1/2}} \left( 1 + \frac{4a^2}{I^2} \frac{1 + \frac{3}{2}I + \frac{3}{8}I^2}{1+I} \right) + O(a^4). \quad (\text{C12})$$

With the aid of (B8), (C9), and (C10) we can show that to second order in  $a$

$$Z(\kappa x_1) = Z(i\kappa) - \frac{i\kappa(4+I)}{I} a^2 [1 + i\kappa Z(i\kappa)], \quad (\text{C13})$$

$$Z(\kappa x_3) = Z(i\kappa(1+I)^{1/2}) + \frac{i\kappa a^2}{I} \frac{4+3I}{(1+I)^{1/2}} \times [1 + i\kappa(1+I)^{1/2} Z(i\kappa(1+I)^{1/2})]. \quad (\text{C14})$$

Insertion of (C9)–(C14) into (C8) yields

$$\frac{\partial A_1}{\partial I} = \frac{A_1(-1 + 2x_1 A_1 + d A_1/x_1)}{d}, \quad (\text{C18})$$

$$\frac{\partial A_3}{\partial I} = \frac{A_3(1 - 2x_3 A_3 + d A_3/x_3)}{d}, \quad (\text{C19})$$

$$\frac{\partial x_k}{\partial I} = -A_k \quad (k=1, 3), \quad (\text{C20})$$

$$\frac{\partial}{\partial I} Z(\kappa x_k) = 2\kappa A_k [1 + \kappa x_k Z(\kappa x_k)] \quad (k=1, 3), \quad (\text{C21})$$

which can be employed in computing the derivative.

<sup>1</sup>P. H. Lee, P. B. Schoefer, and W. B. Barker, Appl. Phys. Lett. **13**, 373 (1968).

<sup>2</sup>V. N. Lisitsyn and V. P. Chebotaev, Zh. Eksp. Teor. Fiz. **54**, 419 (1968) [Sov. Phys. JETP **27**, 227 (1968)].

<sup>3</sup>V. N. Lisitsyn and V. P. Chebotaev, ZhETP Pis. **7**, 3 (1968) [Sov. Phys. JETP Lett. **7**, 1 (1968)].

<sup>4</sup>I. M. Beterov, V. N. Lisitsyn, and V. P. Chebotaev, Opt. Spectrosc. **30**, 497 (1971).

<sup>5</sup>I. M. Beterov, V. N. Lisitsyn, and V. P. Chebotaev, Opt. Spectrosc. **30**, 592 (1971).

<sup>6</sup>M. Gronchi and A. Sona, Riv. Nuovo Cimento **2**, 219 (1970).

<sup>7</sup>V. S. Letokhov, Comments At. Mol. Phys. (GB) **II**, 181 (1971).

<sup>8</sup>A. G. Fox, S. E. Schwarz, and P. W. Smith, Appl. Phys. Lett. **12**, 371 (1968).

<sup>9</sup>A. Szöke, V. Daneu, J. Goldhar, and N. A. Kurnit, Appl. Phys. Lett. **15**, 376 (1969).

<sup>10</sup>N. G. Basov, O. N. Kompanets, V. S. Letokhov, and V. V. Nikitin, Zh. Eksp. Teor. Fiz. **59**, 394 (1970)

[Sov. Phys. JETP **32**, 214 (1971)].

<sup>11</sup>M. S. Feld, A. Javan, and P. H. Lee, Appl. Phys. Lett. **13**, 424 (1968).

<sup>12</sup>A. P. Kazantsev, S. G. Rautian, and G. I. Surdutovich, Zh. Eksp. Teor. Fiz. **54**, 1409 (1968) [Sov. Phys. JETP **27**, 756 (1968)].

<sup>13</sup>S. Stenholm, in *Progress in Quantum Electronics*, edited by J. H. Sanders and K. W. H. Stevens (Pergamon, Oxford, 1971), Vol. 1, Part 4.

<sup>14</sup>H. Greenstein, J. Appl. Phys. **43**, 1732 (1972).

<sup>15</sup>Some preliminary results of this work were presented at the Seventh International Quantum Electronics Conference, Montreal, May, 1972.

<sup>16</sup>S. Stenholm and W. E. Lamb, Jr., Phys. Rev. **181**, 618 (1969).

<sup>17</sup>W. E. Lamb, Jr., Phys. Rev. **134**, A1429 (1964).

<sup>18</sup>If the beam diameters differ in the two cells owing to focusing this can also be included in the parameter  $\alpha$  (see Refs. 4 and 5). Similarly, the effect of collisions can be included in  $\alpha$  (see Sec. V).

<sup>19</sup>For the case of one or two modes, to be discussed here, the indicated division by  $E_n$  can be carried out explicitly. For a general multimode case we may have contributions to  $P_n$  which do not depend on  $E_n$ , and thus the definition is formal only.

<sup>20</sup>The earlier notation  $\hat{t}$  (see Stenholm, Ref. 13) has been replaced by  $t$ , which appears more natural. The physically important point remains  $t = t_f$ . Alternatively we can consider the  $t$  dependence of  $z(t)$  only implicitly and set  $d/dt = \partial/\partial t + v \partial/\partial z$ ; see B. J. Feldman and M. S. Feld, Phys. Rev. A **1**, 1375 (1970); V. M. Fain and Ya. I. Khanin, *Quantum Electronics* (Pergamon, Oxford, 1967), Sec. 25.

<sup>21</sup>In fact, the sum should be replaced by an integral, but because we assume the linewidths of the field to be negligible the integration over a set of discrete frequencies reduces to (2.21). The oscillatory frequencies  $\nu_m$  are assumed to coincide with  $\Omega_m$ , and hence only the combinations of the cold-cavity eigenfrequencies remain.

<sup>22</sup>The simplification affects neither the normalization of

the pumping rates nor the REA results provided that, in the latter case, we regard  $\zeta$  and  $\alpha$  as independent parameters.

<sup>23</sup>When the onset of laser oscillations is regarded as an analog of a phase transition, we have in Fig. 3 the equivalent of a first-order transition.

<sup>24</sup>The relation (3.29) reduces to (3.20) in the limit  $4\kappa^2 \ll I \ll 1/\alpha$  and hence  $\partial H/\partial I$  also vanishes, causing the condition (3.24) to become invalid.

<sup>25</sup>P. T. Bolwijn and C. Th. J. Alkemade, *Physics Lett. A* **25**, 632 (1967).

<sup>26</sup>S. Stenholm, *Phys. Rev. B* **1**, 15 (1970).

<sup>27</sup>W. R. Bennett, Jr., *Phys. Rev.* **126**, 580 (1962).

<sup>28</sup>B. J. Feldman and M. S. Feld, *Phys. Rev. A* **5**, 899 (1972).

<sup>29</sup>S. Stenholm, *Phys. Rev. A* **2**, 2089 (1970).

<sup>30</sup>B. D. Fried and S. D. Conte, *The Plasma Dispersion Function* (Academic, New York, 1961).

<sup>31</sup>*Handbook of Mathematical Functions*, edited by M. Abramowitz and I. Stegun (Dover, New York, 1961), Sec. 7.

## Gas Laser with Saturable Absorber. II. Single-Mode Stability

Rainer Salomaa and Stig Stenholm

*University of Helsinki, Research Institute for Theoretical Physics, Siltavuorenpenger 20 B, SF-00170 Helsinki, 17, Finland*

(Received 26 February 1973)

This paper determines the stability of single-mode operation of a laser with an intracavity absorber. The strong-signal theory for one mode is taken from the previous paper, and the linear response at a different cavity mode is calculated. When its gain exceeds the losses, the chosen operating point is unstable. This determines the regions of stability. The influence of the intensity and position of the strong mode is determined in the rate-equation approximation (REA). The REA is found to follow the exact results rather poorly and an improved approximation (IREA) is given, which at least qualitatively reproduces the structure of the exact gain functions.

### I. INTRODUCTION

The introduction of a saturable absorber cell into the optical cavity of a gas laser provides an efficient method for mode selection.<sup>1-3</sup> If the saturability of the absorber greatly exceeds that of the amplifier, the absorption is bleached at the frequency of a strongly oscillating mode, whereas the unsaturated absorption may suffice to extinguish oscillations over the rest of the amplification band. Thus single-mode operation prevails with only a minor power decrease.

In Paper I<sup>4</sup> we considered the case with identical gases in the cells; the unequal saturability was assumed to be achieved by different amounts of pressure broadening (a simple generalization of the parameters used includes more general situations). We calculated the nonlinear susceptibili-

ties of the polarizable media for single-mode operation with an arbitrary field strength. In this paper we discuss the stability of the hypothesized operating point and determine the parameter ranges where all other modes are damped out.

Two ways of approaching the question of the stability of single-mode operation are available. One can start from steady-state multimode operation and determine the conditions under which this becomes unstable.<sup>5</sup> This requires the solution of a general multimode case—a problem of enormous complexity for strong signals. On the other hand, one can assume single-mode operation and scan the Doppler-broadened gain band with a weak signal.<sup>1,2,6</sup> In the regions where the amplification of the scanning signal is below threshold no self-sustained oscillations can occur. If this is true for all cavity eigenmodes the single-mode solution